Journal of Materials Chemistry C

# Enhancing the Optoelectronic Properties of Solution-Processed AgInSe2 Thin Films for Application in Photovoltaics

| | |
|---|---|
| Journal: | *Journal of Materials Chemistry C* |
| Manuscript ID | TC-ART-09-2023-003540.R1 |
| Article Type: | Paper |
| Date Submitted by the Author: | 23-Nov-2023 |
| Complete List of Authors: | Agarwal, Shubhanshu; Purdue University, Chemical Engineering<br>Weideman, Kyle G; Purdue University, Chemical Engineering<br>Rokke, David; Purdue University, Davidson School of Chemical Engineering<br>Vincent, Kiruba Catherine; Purdue University, Chemical Engineering<br>Zemlyanov, Dmitry; Purdue University, Birck Nanotechnology Center<br>Agrawal, Rakesh; Purdue University, Chemical Engineering |
| | |

ARTICLE

# Enhancing the Optoelectronic Properties of Solution-Processed $AgInSe_2$ Thin Films for Application in Photovoltaics

Received 00th January 20xx,
Accepted 00th January 20xx

DOI: 10.1039/x0xx00000x

Shubhanshu Agarwal,[a] Kyle Weidemann,[a] David Rokke,[a] Kiruba Catherine Vincent,[a] Dmitry Zemlyanov,[b] and Rakesh Agrawal*[a]

$AgInSe_2$ is a promising direct bandgap thin-film material with a rare n-type conductivity. Similar to thin film photovoltaic materials such as $Cu(In,Ga)Se_2$ (CIGSe), which have achieved efficiencies as high as ~23%, $AgInSe_2$ also crystallizes in a chalcopyrite phase while also being more tolerant to antisite defects due to higher defect formation energies resulting from more significant variations in cation sizes. $AgInSe_2$ has a suitable bandgap of 1.24 eV, which lies in the high-efficiency region of the detailed balance limit. In this work, we have utilized a Dimethyl Formamide-Thiourea-Chloride-based solution-processed route to deposit a thin film of $AgInS_2$ which is converted into $AgInSe_2$ after a heat-treatment step in a selenium environment. We observed that $AgInSe_2$ optoelectronic properties depend on the Ag/In ratio and the selenium heat-treatment conditions. Significant improvements in photoluminescence yield and lifetime are observed for Ag-poor films in selenium-rich conditions. X-ray Photoelectron Spectroscopy (XPS) measurements confirm a higher amount of selenium on the surface of films with improved optoelectronic properties. Furthermore, a high minority carrier lifetime of 9.2 ns and a Photoluminescence Quantum Yield (PLQY) of 0.013% is obtained without any passivating layer, which improved to 0.03% after CdS passivation. Hall effect measurements confirm that $AgInSe_2$ has n-type conductivity with a moderate carrier concentration ($10^{-14}$ $cm^{-3}$), more suitable for a p-i-n architecture. XPS has further confirmed the moderate n-type conductivity.

## Introduction

Inorganic semiconductors find utility in various optelectronic applications ranging from photovoltaics to telecommunications, lighting, sensors, medical devices and others.[1–9] For the worldwide use of solar energy to lead to a green energy economy, we need photovoltaic materials that are low-cost, stable, have good optoelectronic and charge transport properties, and can be easily manufactured on a large scale. Thin-film solar cells show all these characteristics, some of which have surpassed the monocrystalline Si efficiency.[10] Among thin-film devices, CdTe and $CuInSe_2$/$Cu(In,Ga)Se_2$ (CISe/CIGSe) are among the most promising. CIGSe has achieved a lab-record efficiency of 23.35% and can be produced by solution processing techniques.[11–13] However, the propensity of copper cations to exist in two oxidation states results in lower formation energy for copper-based defects in the CIGSe crystal lattice.[14–16] Replacing copper with silver in CISe may be helpful as Ag only has a +1 oxidation state and has a larger cation size than $In^{+3}$ and $Ga^{+3}$, significantly increasing the defect formation energy.[17,18] CISe, however, has a bandgap of 1.0 eV, which is not suited for single-junction PV applications, whereas $AgInSe_2$ has a larger bandgap of 1.24 eV, closer to the ideal 1.4 eV bandgap predicted by the detailed balance limit.[19–21] $AgInSe_2$ is also thermodynamically stable and has good electronic properties.[22–24] It is n-type, which is different from CISe/CIGSe, but the structural similarities with CIGSe could be a good sign for the viability of this material. All these favorable properties of silver addition have warranted a need to study $AgInSe_2$ in detail. However, there is only one instance in literature where a solar device has been fabricated from $AgInSe_2$. Agel et al. grew an n-type $AgInSe_2$ film on a p-type Si substrate.[25] They achieved a conversion efficiency of 2.71%, and the device showed Schottky diode-like characteristics. These numbers look promising for a material that has been scarcely studied and optimized.

In most cases, $AgInSe_2$ films have been prepared using costly vacuum processing techniques.[20,23–30] These techniques require a high vacuum, have inefficient material utilization, and involve batch processing.[31,32] Solution processing is a cost-effective alternative for rapidly commercializing promising materials such as $AgInSe_2$. It works at ambient pressure conditions, has a more efficient material utilization, and can be used in the roll-to-roll manufacturing of thin-film absorber films.[33] However, in the literature, there are no reports of a solution-processed $AgInSe_2$ film other than a recent Ph.D. thesis.[34] Limited research has been done on $AgInSe_2$ despite its promising properties. Hence, our research goal is to fabricate a

[a] Davidson School of Chemical Engineering, Purdue University, West Lafayette, Indiana 47907, United States
[b] Birck Nanotechnology Center, Purdue University, West Lafayette, Indiana 47907, United States

Electronic Supplementary Information (ESI) available: [details of any supplementary information available should be included here]. See DOI: 10.1039/x0xx00000x

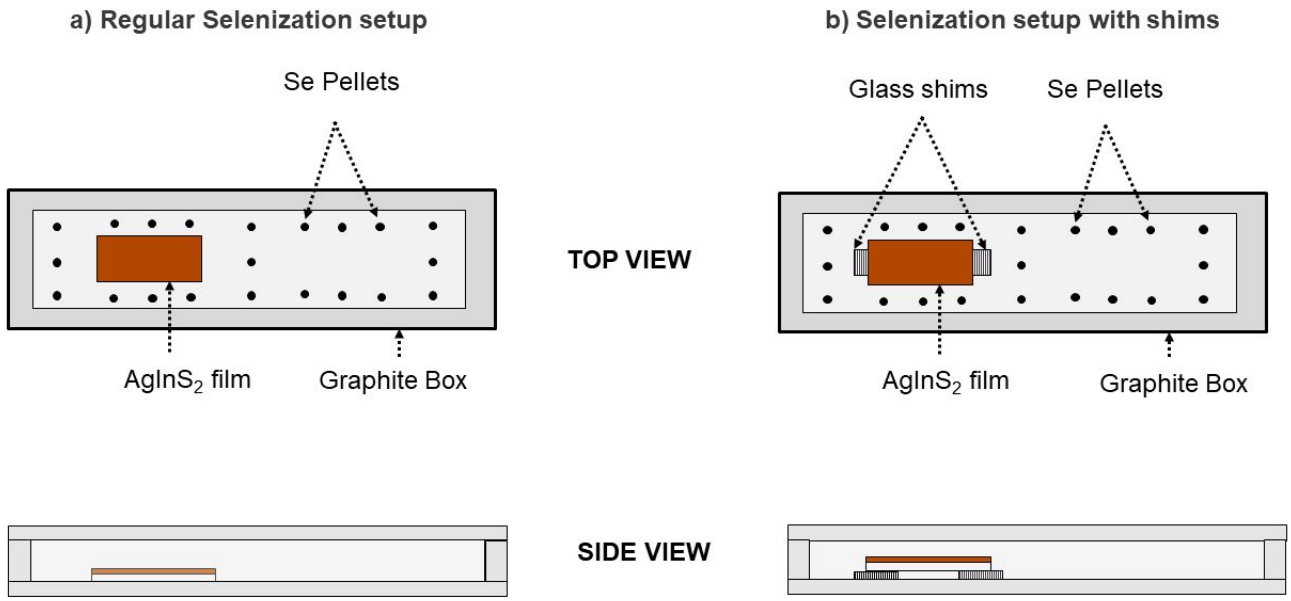


Figure 1 Schematic showing the difference between the (a) regular selenization setup and the (b) selenization setup with shims.

solution-processed $AgInSe_2$ film with good optoelectronic properties for incorporation into a solar cell.

Hence, this work aims to fabricate and characterize solution-processed $AgInSe_2$ films for their potential use in solar cells. We have utilized the benign N-N Dimethyl Formamide (DMF)-Thiourea (TU)-Chlorides chemistry to cast $AgInS_2$ thin film, which is further heat-treated in a selenium environment to form $AgInSe_2$ film. We have optimized the composition and selenization conditions to lower the defects in $AgInSe_2$ films and achieved high Photoluminescence Quantum Yield (PLQY). We have further done advanced characterizations to evaluate the electrical properties and the band positions.

## Experimental

### Materials

Silver (I) Chloride (99.999%), Indium (III) Chloride (99.999%), Thiourea (99.98%), N-N Dimethylformamide (>99.8%), Butylamine (>99.5%), 1,2-Ethanedithiol (>99%), alumina dispersed in 2-propanol (20 wt%), and $SeCl_4$ were obtained from Sigma Aldrich. Selenium used in selenization (5mm pellets, 99.999%) and Selenium powder (99.99%) were obtained from Millipore Sigma. All chemicals were used as received except for the Thiourea, which was twice recrystallized from 18.2 MΩ Deionized Water and dried under vacuum, followed by an ambient-pressure drying in the air overnight at 90°C.

Corning's alkali-free Eagle XG (EXG) glass substrates were obtained from Stemmerich. All chemicals were stored in nitrogen-filled glove boxes.

### Ink Preparation

Ink preparation was performed in a nitrogen-filled glove box. DMF-TU-Chlorides chemistry was utilized to prepare the molecular precursor ink, which uses AgCl and $InCl_3$ as the Ag and In metal precursors. Since AgCl is photosensitive, it was always handled in the dark. In most experiments, 0.8 M total metal concentration was maintained in ink, and the Ag/In ratio was varied. Moreover, 1.6 M TU concentration was maintained in DMF, and AgCl and $InCl_3$ were sequentially added to the TU+DMF solution to prepare the ink. The ink was then vortexed and stirred on a heated stir plate at 35 °C. Before coating, the ink was filtered with a 0.45-micron pore-sized PTFE membrane syringe filter.

A 1.2 M total metal concentration ink was also used with a 3.8 M TU concentration to achieve a relatively thick film.

### Molybdenum and Alumina Deposition

Before molybdenum or alumina deposition, EXG glass was thoroughly rinsed with DI water, 2-propanol, and methanol and then sonicated in an Alconox bath followed by sonication in DI water. The glass was then cleaned in a UV-ozone cleaner for 30 min. The glass was loaded in a PVD chamber for molybdenum deposition and 800 nm thick molybdenum layer was sputtered at an ultralow vacuum.

For film growth on alumina-coated glass, the alumina nanoparticles solution was initially diluted by combining 0.2 ml of commercial alumina solution with 1.8 ml 2-propanol. The solution was then spin-coated on the cleaned EXG glass at 1000 RPM for 1 min, followed by 1 min annealing at 100 $^{o}$C and 30 min annealing at 500 $^{o}$C.

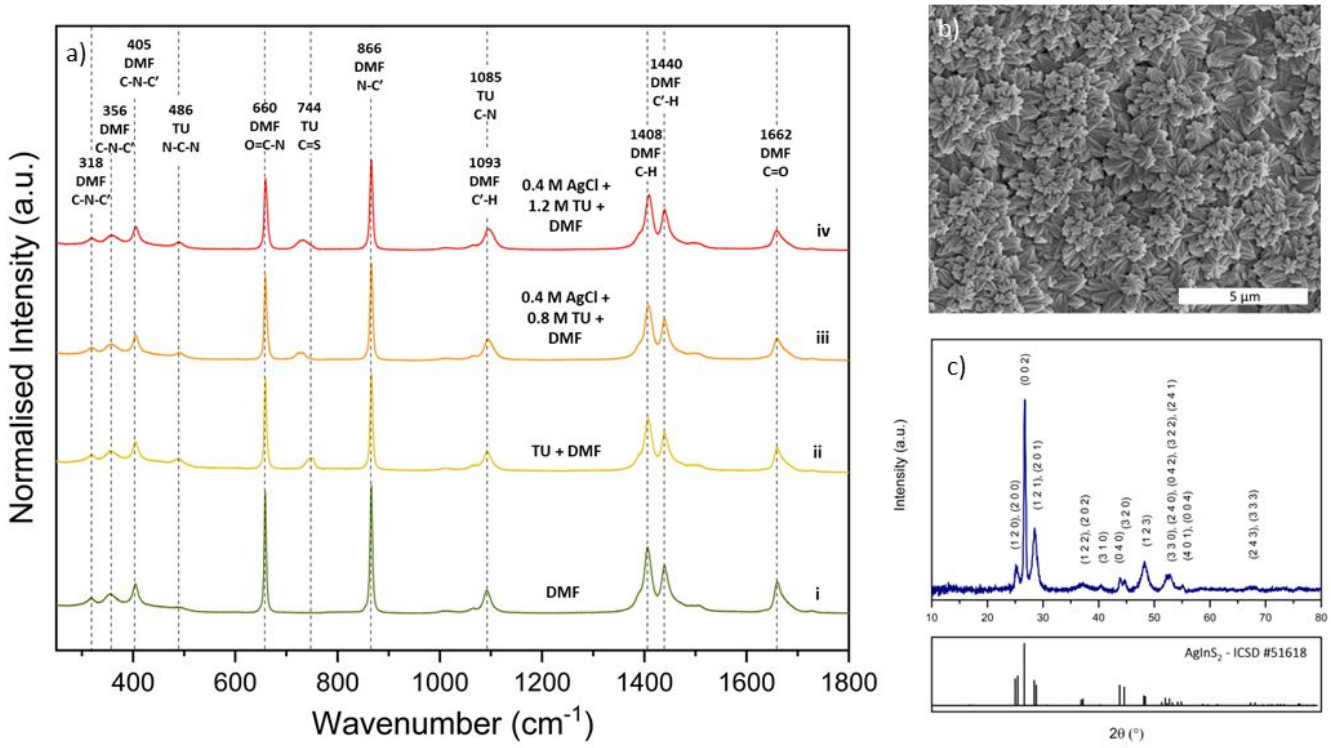


Figure 2 a) Liquid Raman on i) only Dimethyl Formamide (DMF), ii) Thiourea (TU) + DMF, iii) AgCl (0.4 M) + TU (0.8 M) + DMF, iv) AgCl (0.4 M) + TU (1.2 M) + DMF. The peak shift in the C=S bond stretch of TU suggests a metal-sulfur interaction, b) SEM image, c) XRD pattern of as-coated $AgInS_2$ film annealed at 300 °C.

**Film Coating**

The DMF-Thiourea-Chlorides ink was coated on a molybdenum or alumina-coated EXG glass substrate (which contains no sodium) to fabricate $AgInS_2$ thin films. Unless specified, the film is coated on molybdenum in this report. The coating procedure was performed on an automated spin coater in a nitrogen-filled glove box. 200 µl of ink was used in each cycle with the substrate holder rotating at 3000 RPM for 30 seconds, followed by a 30-second wait time for the ink to dry. The sample was then transferred to a hot plate set at 300 °C, and the film was annealed for 90 seconds. The film was then cooled on an aluminum block. This coating cycle was repeated 14 times with 0.8 M total metal concentration ink to achieve a film of the desired thickness. 10 coating cycles with 1000 RPM were used instead with an ink of 1.2 M total metal concentration to achieve thicker films.

**Regular Selenization**

The next step involved annealing the sulfide $AgInS_2$ film in a selenium environment in a refractory tube furnace following the procedure for selenization of $Cu(In,Ga)S_2$ films.[35] In a regular selenization setup, the sample rested on the floor of a graphite box with selenium pellets arranged around it, as shown in **Figure 1a**. Before ramping up the temperature, the tube furnace was purged multiple times through vacuum and argon cycles to remove the oxygen. Then, the furnace temperature was ramped up to the desired setpoint (475-600 °C), and the film was annealed in a selenium environment for 20 minutes.

**Modified Selenization with glass shims**

A modified selenization setup was used to increase the selenium supply to the film during the heat-up period. In this setup, the sample rested on two small pieces of EXG glass near the far edges of the 1" x 0.5" film, shown in **Figure 1b**. This arrangement avoided any direct contact of the sample with the graphite box, which has high absorptivity and thermal conductivity and thus quickly heats the sample if it rests directly on the graphite surface. However, the selenium pellets were still in contact with the graphite floor and volatilized normally, the volatility rate set by the graphite floor temperature. The sulfide film heated up slowly because of increased thermal resistance from the glass shims, resulting in a significant difference in temperature between the selenium vapors and the film's surface, causing higher selenium condensation onto the film. Hence, this modified setup had more liquid Se on the film. Simplified numerical heat transfer calculations in **Figures S1 and S2** and Weidemann's doctoral thesis support the above discussion.[36]

**Other Selenization Methods**

Other selenization methods with higher selenium availability were also employed. In the first case, an additional 0.4 M selenium ink in Butylamine + 1,2-Ethanedithiol was prepared, and two layers of this ink were coated on top of the $AgInS_2$ film. The film was then annealed at 100 °C for two minutes to remove the solvents. This provided a thick layer of Se on the $AgInS_2$ film that could act as a selenium source

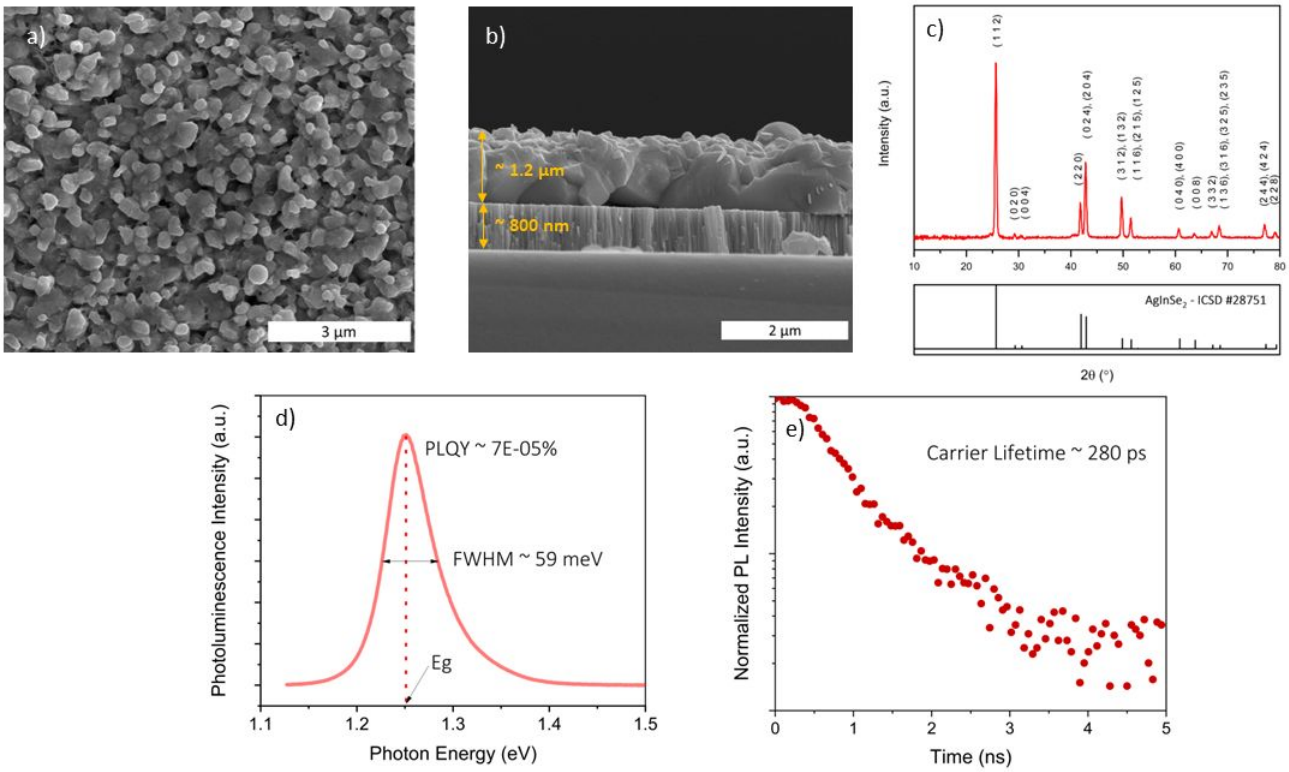


Figure 3 a) SEM top-view, b) SEM cross-sectional view, c) XRD pattern, d) Photoluminescence plot, and e) TRPL decay curve of stoichiometric $AgInSe_2$ film selenized at 500 °C with regular selenization (arrangement shown in Figure 1a).

during selenization. This modified film was further selenized by regular selenization (no shims used). In another method, 25 mg selenium powder was spread on the $AgInS_2$ film, which also acted as the selenium source during selenization. This film was also selenized via regular selenization.

**CdS Deposition**

CdS was deposited using chemical bath deposition as reported elsewhere.[37]

**Characterization**

Raman spectroscopy was performed using a Horiba/Jobin-Yvon HR800 Raman spectrometer with a 632.8 nm excitation laser wavelength. A quartz cuvette enclosed in a nitrogen atmosphere was used for collecting spectra on liquid solutions. X-ray diffraction was performed in a Rigaku SmartLab Diffractometer under ambient conditions in parallel beam geometry with an incident beam angle of 0.5 degrees using a Cu Kα source (λ = 1.5406 Å) operating at 40 kV and 44 mA. Hall effect measurements were performed on a LakeShore M91 FastHall with magnetic field strengths from -9 Tesla to 9 Tesla.

Time-resolved photoluminescence (TRPL) was acquired by the single photon counting technique using a 640 nm diode laser (pulse width of 100 ps, 1 MHz) and an InGaAs photomultiplier tube (Hamamatsu H10330-75). The obtained TRPL decay curves were fitted with biexponential fits, and the statistical average of the lifetime values was reported. The statistical average is given by:

$$\tau_{stat} = \frac{B_1\tau_1 + B_2\tau_2}{B_1 + B_2}$$

$B_1$ and $B_2$ are the pre-exponential factors, and $\tau_1$ and $\tau_2$ are the characteristic minority carrier lifetimes.

Photoluminescence measurements were performed with a Horiba LabRAM HR800 using a 632.8nm He:Ne laser and a liquid nitrogen-cooled InGaAs detector. Spectral corrections were performed by comparing the normalized measured spectrum of a calibrated light source (Avantes Avalight HAL-CAL MINI) with the known normalized spectrum provided by the vendor, as detailed in a previous report.[38] Further apparatus calibration was performed to obtain quantitative photoluminescence, as detailed in Rokke's doctoral thesis.[34]

The XPS data was obtained at the Surface Analysis Facility of the Birck Nanotechnology Center, Purdue University. X-ray photoelectron spectroscopy (XPS) measurements were performed using a Kratos

Axis Ultra DLD imaging XPS instrument with a monochromatic Al Kα (1486.6 eV) radiation and a chamber pressure of less than 2E-09 Torr. The samples were transferred immediately to an argon-filled glovebox after selenization to avoid oxygen contamination and were then vacuum sealed to transfer to the XPS instrument. The vacuum seal was broken inside a glovebox connected to the XPS instrument. For the XPS data analysis CASAXPS software was used. The data was charge corrected using the C1s peak set at 284.8 eV.

Scanning electron microscopy (SEM) measurements were performed on the FEI Quanta three-dimensional system with an Everhart-Thornley detector at an accelerating voltage of 7 kV with a working distance of 10 mm.

Fisher XAN 250 X-ray fluorescence (XRF) instrument at 50 kV voltage with a primary Ni filter containing a silicon drift detector was used to measure the bulk composition. We have reported XRF-measured composition rather than the nominal composition in this work.

Reflectance data was acquired using a Perkin-Elmer Lambda 950 spectrometer with an integrating sphere.

## Results and Discussions

### Solution-Processed $AgInSe_2$

In the only reported case of solution-processed $AgInSe_2$ film, $Ag_2S$ and In as the metal precursors were dissolved in Butylamine and 1,2-Ethanedithiol to prepare a stable ink.[34] However, this approach had some challenges: a) the films had a poor PL yield, b) their minority carrier lifetime was low at around 300 ps, and c) the amines and thiols are toxic.

All the above challenges motivated us to search for other benign chemistries. We explored the DMF-Thiourea-Chlorides route, which is reported to produce carbon-free $CuInSe_2$ thin films.[16] DMF, a Lewis basic aprotic solvent, cannot solvate monovalent cations, such as $Ag^+$, on its own. However, adding TU stabilizes the $Ag^+$ cation, and the solubility of AgCl increases when at least two mol of TU are present per mol of AgCl. The 0.4 M AgCl with 0.4 M TU in DMF did not dissolve. However, 0.4 M AgCl dissolved completely with 0.8 M and higher TU concentrations in DMF. Liquid Raman measurements verify an interaction of AgCl and TU owing to the gradual peak broadening and peak shift of the 744 $cm^{-1}$ C=S stretch, as shown in **Figure 2a**. Thiourea also increases the solubility of $InCl_3$ by reacting with the free $Cl^-$ in the solution and increasing the concentration of highly soluble $[InCl]^{2+}$ species.[16] **Figures 2b** shows the as-coated $AgInS_2$ films from the equimolar AgCl and $InCl_3$ ink which form densely packed flower-shaped grains via this route and showed the orthorhombic phase as opposed to the chalcopyrite phase observed in the literature at these temperatures, see **Figure 2c**. Surprisingly, the as-coated film showed an intense PL emission with a broad spectrum centered at 1.18 eV, possibly originating from a midgap defect in $AgInS_2$ or some secondary phases, as evidenced by **Figure S3**. We performed the variable temperature photoluminescence (PL) for the as-coated $AgInS_2$ film at 150 K and 77 K and observed the similar midgap peak with increased intensity as the measurement temperature reduced (**see Figure S4**). We also observed a slight blue shift in the midgap PL peak position as the temperature reduced. However, still more work is required on assigning this peak as the room-temperature PL peak position changes slightly from one spot to another varying between 1.17 to 1.25 eV, as shown in **Figure S5**.

**Figure 3c** indicates the as-coated stoichiometric orthorhombic $AgInS_2$ film converted to chalcopyrite $AgInSe_2$ film after selenization. We potentially accessed a selenium rich Ag-Se binary alloy liquid flux that helped nucleate and grow large $AgInSe_2$ grains similar to those reported for other material systems.[39–41] The selenized film has irregularly shaped grains when selenized with regular selenization conditions, as shown in **Figures 3a** and **3b**. **Figure S6** shows the film also has residual carbon. Different values have been reported in the literature for the bandgap of $AgInSe_2$ ranging between 1.02 to 1.35 eV depending on the growth method and processing conditions.[20,24,25,27,28,30,42–47] However, the photoluminescence for our film is centered at 1.25 eV with a narrow FWHM of 59 meV, shown in **Figure 3d**. The bandgap was further confirmed by the Kubelka-Munk transformation on UV-vis-NIR diffuse reflectance measurement. The analysis in **Figure S7** shows that the optical bandgap of the film is 1.24 eV which is comparable to the photoluminescence peak position. The PLQY yield and the minority carrier lifetimes were poor for the stoichiometric film under all conditions of regular selenization with PLQY less than 1E-04% and a lifetime less than 300 ps, shown in **Figures 3d** and **3e**. We tried selenizations at temperatures between 475 and 525 $^oC$ but saw no improvements. These results suggest the presence of intrinsic defects in the $AgInSe_2$ fabricated under these conditions.

### Effect of Ag/In ratio on the Optoelectronic Properties of $AgInSe_2$

We also varied the Ag/In ratio in the solution-processed $AgInSe_2$ films produced via the DMF-Thiourea-Chlorides chemistry to study its impact on optoelectronic properties. For Ag/In<1 (Ag-poor), we observed slight improvements in PL and lifetime similar to CISe/CIGSe. These improvements continued for Ag/In as low as 0.9, where they started forming a secondary phase of $AgIn_5Se_8$, as shown in **Figure 4a**. Although there was an improvement in PL and carrier lifetime, the numbers were still relatively low, as shown in **Figure 4b**. These improvements were possibly due to the formation of benign defect complexes for Ag-poor films, such as $2V_{Ag}+In_{Ag}$, similar to those reported for $CuInSe_2$.[48] While Ag poor $AgInSe_2$ composition seems favorable, other defects may also limit the performance.

### Annealing $AgInSe_2$ in Se Rich Atmosphere

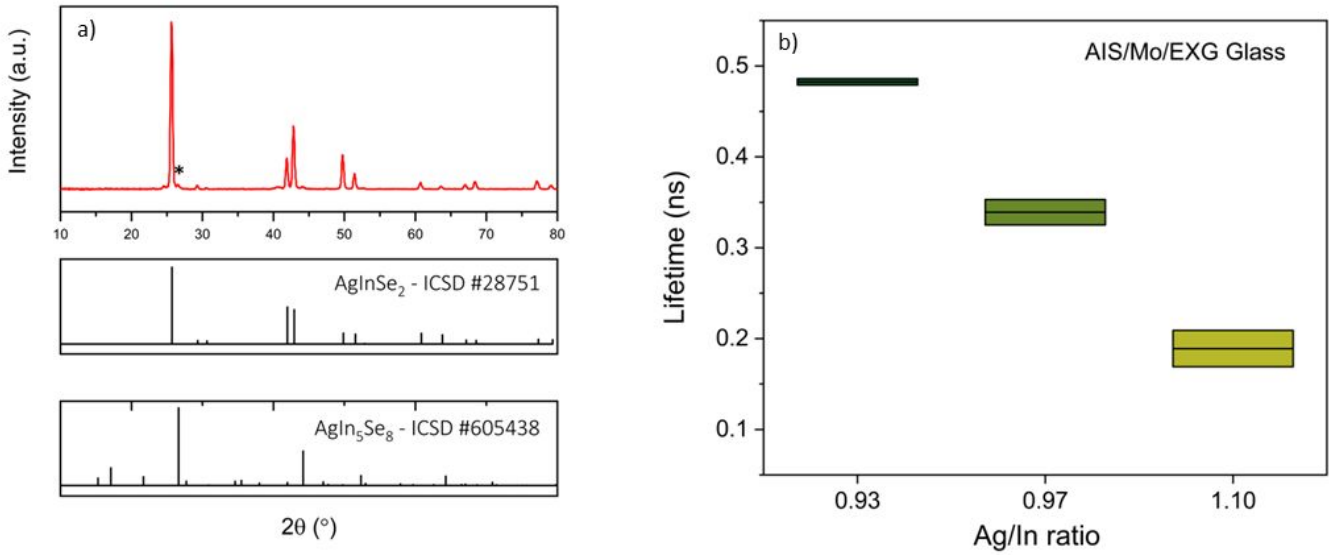


Figure 4 a) XRD pattern of $AgInSe_2$ film with Ag/In ~ 0.87 (* indicate $AgIn_5Se_8$ peak), b) Plot showing the variation of $AgInSe_2$ carrier lifetime with Ag/In ratio in the films selenized at 500 $^oC$ with regular selenization.

The published literature on $AgInSe_2$/$CuInSe_2$/Cu(In,Ga)$Se_2$ has many instances of the detrimental effects of selenium vacancies on the absorber films. In a few cases, authors noted that growing $AgInSe_2$ in a Se-deficient environment could harm the material's crystallinity and electronic properties. Ema et al. observed that the phase pure chalcopyrite $AgInSe_2$ could only be produced when sufficient Se vapor was provided.[49] Patel et al. found that the $AgInSe_2$ films exhibited higher resistivity because of selenium deficiency.[26] On similar grounds, Matsuo et al. pointed out that the $AgInSe_2$ samples annealed above 400 $^oC$ contained Ag and Se vacancies ($V_{Ag}$ and $V_{Se}$, respectively).[28] In $CuInSe_2$, selenium vacancies act as donors and provide electrons to the conduction band; similar phenomena may happen for $AgInSe_2$. In this regard, Abdel-Hady et al. noticed that the room temperature electron concentration varied between $10^{12}$-$10^{18}$ $cm^{-3}$ based on selenium deficiency for their n-type $AgInSe_2$ film.[23] Thus, it is apparent that growing $AgInSe_2$ in a selenium-deficient environment could be deleterious.

The above discussion points towards that $V_{Se}$ defects could potentially be harmful to the $AgInSe_2$ absorber films. Hence, we hypothesized that the photoluminescence yield and minority carrier lifetime in solution-processed $AgInSe_2$ would improve by increasing the selenium availability during selenization. Thus, our goal was to increase the selenium flux and maintain a selenium-rich environment during selenization to minimize defect formation while limiting the excess condensed selenium vapor on the final film.

We used various means to incorporate increased selenium in the films to test our hypothesis. Methods include using glass shims as the support for the substrate to increase selenium condensation on the film (**Figure 1b**), coating Se layers on top of as-coated $AgInS_2$, and dusting Se powder on $AgInS_2$ film before selenization. These methods are discussed in detail in the experimental section.

**Improvements in Optoelectronic Properties**

The majority of literature noted $AgInSe_2$ to be an n-type material. Moreover, similar to $CuInSe_2$, $V_{Se}$ could be a deep donor defect in $AgInSe_2$, which can act as recombination centers for minority carrier holes. If present in a high concentration, $V_{Se}$ could harm the optoelectronic properties. Hence, we focused on incorporating increased selenium in the film during selenization.

**Selenization on glass shims** During initial heat-up period, selenium is at a higher temperature than the $AgInSe_2$ film. Thus, selenizing the $AgInSe_2$ film on glass shims instead of directly on the graphite box floor would cause more selenium condensation on the film during the initial heat-up period and should help passivate the selenium-based defects. **Figures 5a** and **5b** confirm the hypothesis as both the PL and lifetime improved with shims. Using this modified selenization setup, we achieved a minority carrier lifetime of around ~ 800 ps for a $AgInSe_2$ film with Ag/In ~ 0.97 compared to ~ 300 ps for the regular selenization with the same metal composition; the PL Yield (the area under the PL peak) also improved. We noted an increasing trend in lifetime and PL as the Ag/In ratio in the films decreased (**Figures 5c** and **5d**), as observed previously for the films selenized without shims. However, the PL intensities and lifetime values were much higher with shims, and we observed a high lifetime of ~ 1.6 ns for Ag/In ~ 0.91. Since higher selenium availability is causing these improvements, other methods (described in the experimental section) were also tested to increase the selenium availability during selenization. Raman mapping conducted on films selenized on shims only indicated the presence of $AgInSe_2$ based on 50 different Raman peaks, however, variations in relative peak intensity were present owing to discontinuities in the film (see **Figure S8**). We further note that in the temperature range of 475 $^oC$ to 515 $^oC$, we did not observe any clear trend in the PL yield and lifetime with the selenization temperature when the samples were selenized on shims, evidenced

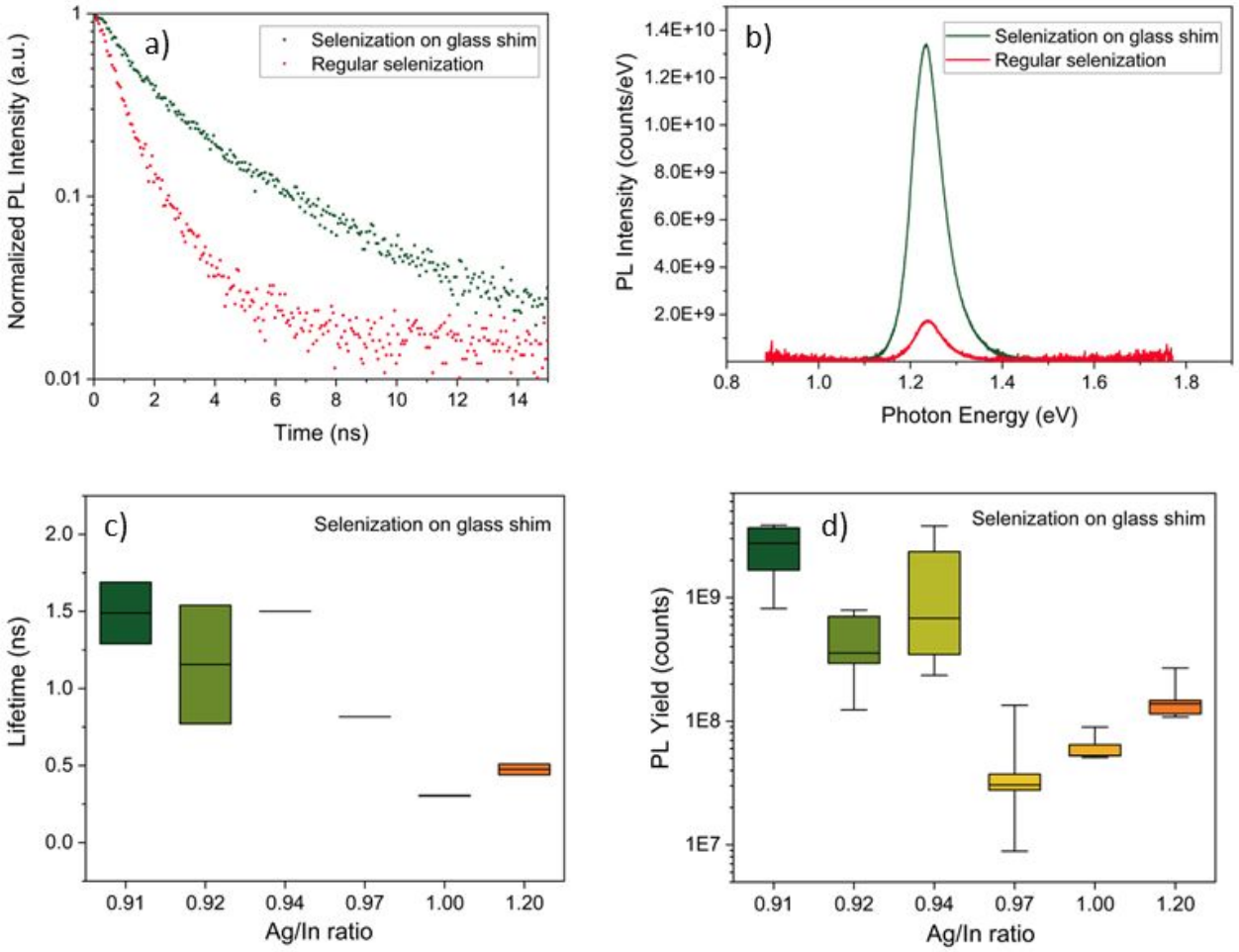


Figure 5 a) Difference in the TRPL decay curves, b) Difference in PL intensities for the $AgInSe_2$ film selenized on shims and the film selenized without shims at 500 $^oC$ with Ag/In ~ 0.92, c) Plot showing the variation in the carrier lifetime, and d) Plot showing the variation in the PL yield for the $AgInSe_2$ films with Ag/In ratio selenized at 500 $^oC$ using shims. The film stack is $AgInSe_2$/Mo/EXG Glass.

in **Figure S9**. This observation can be attributed to two opposing phenomena, grain growth, and selenium loss. We believe the grains would grow more significantly with higher selenization temperature which should contribute to reducing the number of grain boundary interfaces, possibly reducing the interaction of charge carriers with potential grain boundary defects and lowering the non-radiative recombination. This should, in turn, increase the PL yield and the carrier lifetime. However, a higher selenization temperature volatilizes and loses the available selenium faster due to its higher vapor pressure. This may cause some of the selenium from the film to volatilize, leading to selenium-based defects. These two competing effects possibly cause no trend in the lifetime with the selenization temperature.

**Incorporating Increased Selenium via Different Methods** Since we started observing a secondary phase of $AgIn_5Se_8$ around 0.9, we used Ag/In ~ 0.93 for the other characterizations on the $AgInSe_2$ films in this report. As described in the experimental section, we tested two other methods to incorporate increased selenium, first by sprinkling ~ 50 mg selenium powder and another by coating two layers of selenium ink on the top of 0.5" x 1" as-coated sulfide film. We then selenized these films without shims using regular selenization at 600 $^oC$. In both these cases, the photoluminescence yield was comparable to the film selenized on shims at the same conditions without any added selenium on top of the sulfide film (**Figure 6a)**. Moreover, the PL yield in both cases was much higher than the regular selenization without extra selenium incorporation. These results support our hypothesis that increased selenium supply benefits $AgInSe_2$ irrespective of the supply method used.

**Alumina as the Back Layer** In order to further increase the selenium condensation, DMF-TU-Chlorides ink was coated on an alumina-coated glass substrate instead of a molybdenum-coated glass substrate. The alumina has poorer heat transfer properties than the molybdenum, which slowed down the heat transfer to the film, driving higher selenium condensation. The alumina layer also has the propensity to prevent rapid nucleation and growth on its surface, resulting in top-down growth.[50] The results further confirm our

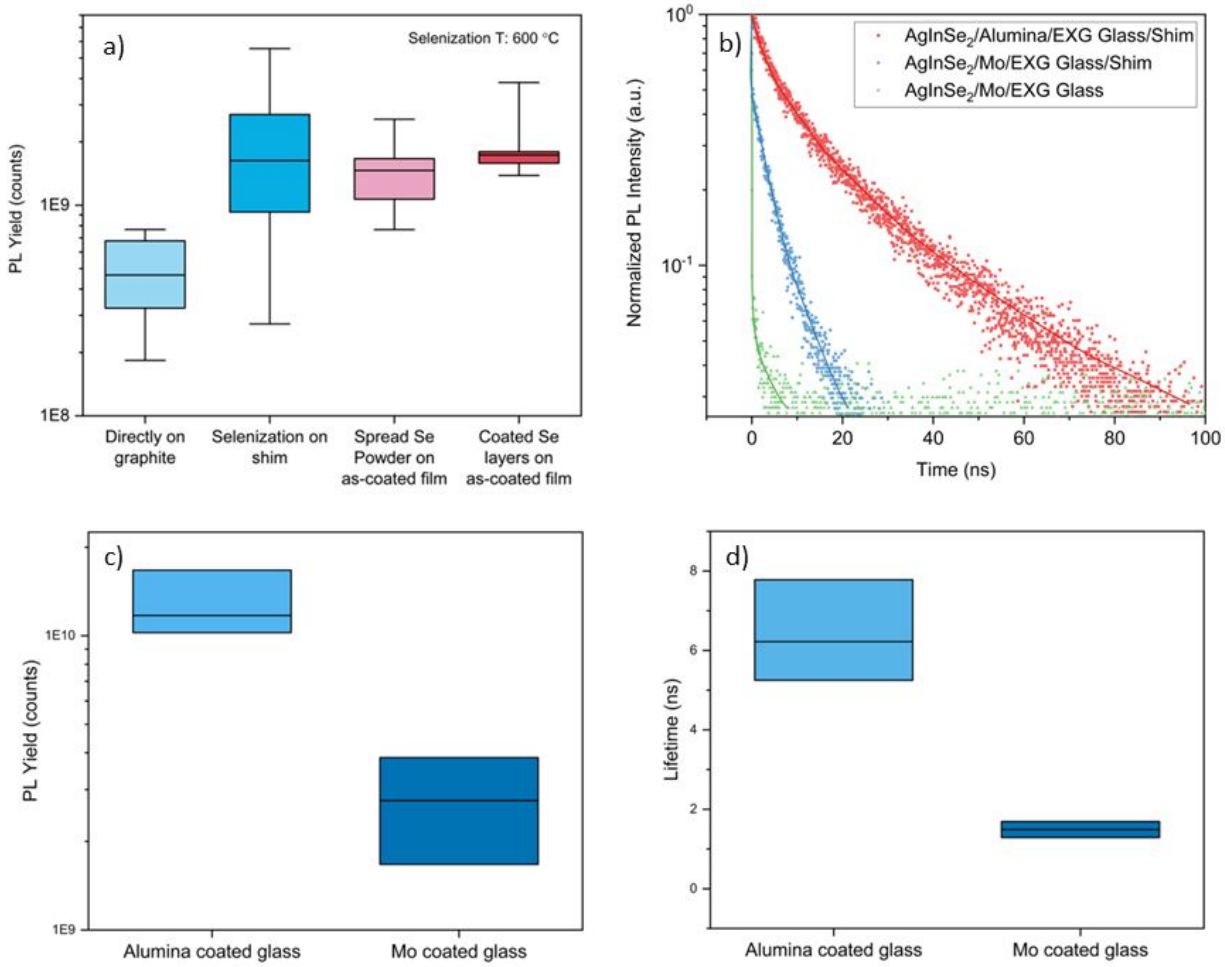


Figure 6 a) PL intensities for the different selenization approaches for $AgInSe_2$ films selenized at 600 °C, b) TRPL decay curves for the $AgInSe_2$ films selenized at 515 °C on shims with Alumina and Molybdenum at the back, c) Carrier lifetime and d) PL yield for the $AgInSe_2$ films selenized with shims at 515 °C with Alumina and Molybdenum at the back respectively. These $AgInSe_2$ films have an Ag/In ~ 0.93.

hypothesis as the photoluminescence yield and lifetime improved significantly with the alumina at the back of the film, as shown in **Figures 6c and 6d**. **Figure 6b** compares the TRPL decay curves for the best films in the three cases, and the $AgInSe_2$ film on alumina-coated glass is superior. A high carrier lifetime of 9.22 ns was achieved for the film selenized using shims with alumina at the back. Theoretical $V_{oc}$ calculations were also performed using the intensity-dependent Photoluminescence Quantum Yield (PLQY) calculations extrapolated to 1-sun. The film selenized on shims at 515 °C for 20 minutes achieved a high PLQY of 0.0128% (see **Figure S10**) and subsequently high theoretical $V_{oc}$ of around 732 mV compared to 600 mV achieved for the film selenized directly on the graphite surface. It is worthwhile to note that we achieved these high numbers on the bare absorber film without any surface passivation. Without optimizing, we deposited a 50 nm layer of CdS via chemical bath deposition on the absorber film, and the PLQY improved to 0.03%, achieving a theoretical $V_{oc}$ of 754 mV (detailed curves in **Figures S11 and S12**). We believe these improvements are caused by the reduction of surface states and dangling bonds suppressing the surface recombination as reported for other materials.[51] $V_{oc}$ is a critical device parameter, and a $V_{oc}$ above 700 mV is required for high-efficiency devices with a bandgap of around 1.2 eV. Also, this high PLQY suggests a maximum theoretical device efficiency of around 18%, inferred from the efficiency vs. PLQY% plot published elsewhere for different photovoltaic materials.[52] We further performed the variable temperature photoluminescence (PL) for the selenized $AgInSe_2$ film at 150 K and 77 K and observed that the PL intensity and the FWHM improves as the temperature is reduced, see **Figure S13**. We also didn't observe any defect peak. Hence, these results look promising for $AgInSe_2$.

**XPS Measurements Confirm Surface Selenium Amounts** We observed improvements in PL yield and lifetime whenever attempts were made to incorporate selenium in increased amounts. However, XRF, which has a precision of 0.5 at%, measured the same bulk selenium composition for all the samples. To verify the surface selenium content in the film, we conducted XPS analysis, which has a detection limit of approximately 0.1 at%. XPS data were collected from the Ag3d, In3d, and Se3d regions of both the film selenized on shims and film selenized directly on graphite. The XPS spectra are

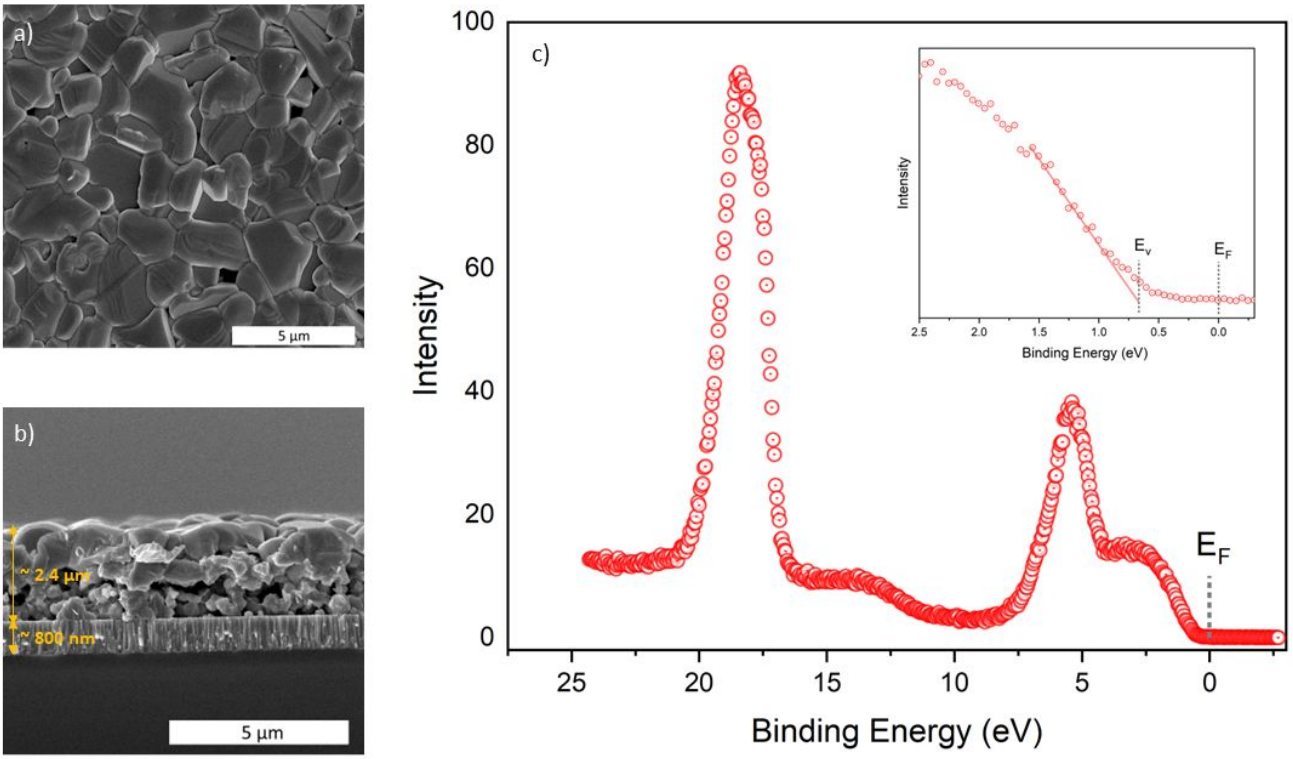


Figure 7 a) SEM top-view, and b) SEM cross-sectional view of $AgInSe_2$ film prepared from 1.2 M conc. ink with Ag/In ~ 0.93 and selenized at 600 °C using shims, c) Valence band spectra for $AgInSe_2$ film prepared from 1.2 M conc. ink with Ag/In ~ 0.93 and selenized at 600 °C. The position of the valence band edge with respect to the Fermi level is marked.

presented in **Figure S14**. The XPS analysis indicated a higher selenium content on the film's surface that was selenized on shims compared to the film selenized on graphite (**Table 1)**. However, the bulk composition measured by the XRF remains nearly the same. This suggests a potential loss of selenium from the surface and near-surface regions, which may be affecting the optoelectronic properties.

Table 1 Comparison of the surface and bulk compositions of $AgInSe_2$ films selenized on graphite and selenized on shim analyzed by XPS and XRF, respectively.

| | **$AgInSe_2$ selenized on graphite** | **$AgInSe_2$ selenized on shim** |
|---|---|---|
| **Surface Composition (XPS)** | $Ag_{0.64}In_1Se_{1.2}$ | $Ag_{0.52}In_1Se_{1.5}$ |
| **Bulk Composition (XRF)** | $Ag_{0.94}In_1Se_{2.3}$ | $Ag_{0.92}In_1Se_{2.3}$ |

**Continuous Film Formation**

Till now, we have achieved excellent optoelectronic properties for $AgInSe_2$ films, but the films are rather non-homogenous, as shown in **Figures S15, S16, S17, and S18**. They have large disconnected grains, possibly because of the excessive growth in the out-of-plane direction. Hence, there was a need to achieve a thicker film so that grains grow enough laterally and a continuous film is achieved. We achieved a relatively continuous film using shims after selenization when started with 1.2 M total metal concentration, coated 10 layers and selenized at 600 °C, as shown in **Figures 7a and 7b**. However, we only achieved an estimated $V_{oc}$ of 700 mV for this film through PLQY analysis, which was slightly lower than the films selenized at lower temperatures. This is partially due to the inability to maintain a saturated selenium environment at 600 °C for 20 min due to the high vapor pressure of selenium and, therefore, increased selenium leakage rate from the box during annealing and cool down. We again connect this to the selenium-based defects. The grain size improved upon selenization at higher temperatures, which should have reduced the grain boundary recombination, but some other defects seem to affect the performance of higher-temperature films. We hypothesize that increased selenium loss from the film at higher temperatures could limit the performance. In other words, selenium vacancies were possibly formed in $AgInSe_2$ film by selenizing at higher temperatures in an insufficient selenium environment and during cooldown. Nonetheless, we again passivated this film with a 50 nm thick layer of CdS, and it improved the $V_{oc}$ to 741 mV with a PLQY of 0.019%.

**Electrical Characterizations**

These has been a lack of consensus on the electrical properties of $AgInSe_2$ in the literature. Both p-type and n-type conductivity has been suggested for $AgInSe_2$ with carrier concentrations varying from intrinsic to $10^{18}$ $cm^{-3}$. Similar large variations have also been reported for the conductivity and the carrier mobility.[23,24,26–28,30,44–46,49] These variations might be due to the different defects being present in the material depending on the composition. It is possible that the selenium vacancies are contributing to the n-type conductivity and a selenium poor composition may lead an n-type conductivity with high electron concentration. Other possibility is that $In_{Ag}$ defect might be a shallow donor defect and could be contributing electrons to the conduction band, although more work is needed to confirm this. Similarly, Ag vacancies will possibly contribute to the p-type conductivity. Hence, a silver poor and selenium rich composition may lead to p-type conductivity. Moreover, the grain size and the continuity of the film may affect the conductivity and the carrier mobility as the grain boundaries are often defective. Nonetheless, we performed Hall effect measurements in Van der Pauw configuration to determine the parameters for our continuous film. We swept the magnetic field from –9 to 4 T and recorded the room temperature Hall voltage, shown in **Figure S19**. On data analysis, we obtained an n-type conductivity for the $AgInSe_2$ film with a moderate carrier concentration of $10^{14}$ $cm^{-3}$, low carrier mobility of 1.2 $cm^2/V.s$ and high resistivity of 520 ohm-m. The low carrier mobility and high resistivity could possibly be because of the thick fine grain layer at the bottom of the film and a moderate carrier concentration limiting the number of carriers available for conduction. Future work could look into eliminating the thick fine grain layer at the bottom to improve the carrier properties. The XPS measurements near the valence band maximum further confirmed the n-type conductivity. The analysis suggests an energy gap of 0.68 eV between the Fermi-level ($E_F$) and the valence edge position ($E_V$), whereas the bandgap is 1.25 eV, see **Figure 7c**. Both p-n and p-i-n heterojunctions may be possible for these moderate carrier concentrations. However, the choice of hole and electron transport layers is not immediately obvious.

We further tried to match various materials with the band positions reported for $AgInSe_2$ for the electron and hole transport layers.[53] CdS has a significant conduction band offset (~ 0.35 eV) with $AgInSe_2$, whereas $NiTiO_3$ has a conduction band offset of ~ 0.15 eV.[54,55] On the other hand, MnS has a suitable valence edge location with high hole concentration and could be a viable option for the hole transport layer.[53] Future work will explore the p-i-n architecture for $AgInSe_2$ using the materials mentioned earlier and other novel hole and electron transport layers to fabricate a solar device.

## Conclusions

$AgInSe_2$ is a promising photo absorber with a high absorption coefficient, suitable bandgap, and n-type conductivity. We implemented the DMF-TU-Chlorides chemistry to synthesize a high-quality solution-processed $AgInSe_2$ thin film. Our study shows that selenium-based defects harm $AgInSe_2$ and seriously affect optoelectronic properties. A careful study was performed to incorporate increased selenium during the heat treatment by maintaining high thermal gradient between the selenium vapors and the surface of the film resulting in the increased condensation of selenium on the film. This increased incorporation of selenium improved the optoelectronic properties and we achieved a lifetime of 9.2 ns, PLQY of 0.013%, and a theoretical estimated $V_{oc}$ of 732 mV without surface passivation. Further improvements in the photoluminescence were observed after passivation with CdS. These exciting optoelectronic properties motivate to synthesize an $AgInSe_2$-based solar cell but moderate carrier concentration of $10^{14}$ $cm^{-3}$ measured from the Hall effect measurements suggest that the p-n heterojunction may not be suitable for this low carrier concentration, requiring consideration of alternate architectures such as p-i-n solar cells.

## Author Contributions

Shubhanshu Agarwal: Conceptualization, investigation, methodology, visualization, writing – original draft. Kyle Weidemann: Methodology, formal analysis (Hall effect measurements). David Rokke: Conceptualization, Writing – review & editing. Kiruba Catherine Vincent: Formal analysis (Raman mapping), Writing – review & editing. Dmitry Zemlyanov: formal analysis (XPS measurements). Rakesh Agrawal: Funding acquisition, project administration, supervision, resources, writing – review & editing.

## Conflicts of interest

There are no conflicts to declare.

## Acknowledgements

The authors are grateful for the financial support from the National Science Foundation through Grants 1735282-NRT (SFEWS) and 10001536 (INFEWS). The authors would like to thank Jonathan Turnley, Apurva Pradhan, and Dr. Alexei Lagoutchev for their valuable discussions related to the project. The XPS data were obtained at the Srface Analysis Facility of the Birck Nanotechnology Center at Purdue University.

## References

(1) Sahoo, D.; Naik, R. A Review on the Linear/Nonlinear Optical Properties of Se Doped Chalcogenide Thin Films as Potential Optoelectronic Applications. J Non Cryst Solids 2022, 597, 121934. https://doi.org/10.1016/j.jnoncrysol.2022.121934.

(2) Mishra, N.; Vasavi Dutt, V. G.; Arciniegas, M. P. Recent Progress on Metal Chalcogenide Semiconductor Tetrapod-Shaped Colloidal Nanocrystals and Their Applications in Optoelectronics. Chemistry of Materials 2019, 31 (22), 9216–9242. https://doi.org/10.1021/acs.chemmater.8b05363.

(3) Goumri-Said, S.; Shah, M. A.; Azam, S.; Irfan, M.; Kanoun, M. B. Investigation of Electronic and Optical Properties of the Ternary Chalcogenides for Optoelectronic Applications: A TB-MBJ DFT Study. Current Applied Physics 2023, 49, 151–157. https://doi.org/10.1016/j.cap.2023.02.021.

(4) Priyadarshini, P.; Das, S.; Naik, R. A Review on Metal-Doped Chalcogenide Films and Their Effect on Various Optoelectronic Properties for Different Applications. RSC Adv 2022, 12 (16), 9599–9620. https://doi.org/10.1039/D2RA00771A.

(5) Xia, C.; Li, J. Recent Advances in Optoelectronic Properties and Applications of Two-Dimensional Metal Chalcogenides. Journal of Semiconductors 2016, 37 (5), 051001. https://doi.org/10.1088/1674-4926/37/5/051001.

(6) Wang, M.; Zhuang, X.; Liu, F.; Chen, Y.; Sa, Z.; Yin, Y.; Lv, Z.; Wei, H.; Song, K.; Cao, B.; Yang, Z. New Approach to Low-Power-Consumption, High-Performance Photodetectors Enabled by Nanowire Source-Gated Transistors. Nano Lett 2022, 22 (23), 9707–9713. https://doi.org/10.1021/acs.nanolett.2c04013.

(7) Liu, D.; Chen, R.; Liu, F.; Zhang, J.; Zhuang, X.; Yin, Y.; Wang, M.; Sa, Z.; Wang, P.; Sun, L.; Pang, Z.; Tan, Y.; Jia, Z.; Chen, M.; Yang, Z. Flexible Omnidirectional Self-Powered Photodetectors Enabled by Solution-Processed Two-Dimensional Layered $PbI_2$ Nanoplates. ACS Appl Mater Interfaces 2022, 14 (41), 46748–46755. https://doi.org/10.1021/acsami.2c13373.

(8) Park, G. S.; Lee, S.; Kim, D.; Park, S. Y.; Koh, J. H.; Won, D. H.; Lee, P.; Do, Y. R.; Min, B. K. Amorphous $TiO_2$ Passivating Contacts for $Cu(In,Ga)(S,Se)_2$ Ultrathin Solar Cells: Defect-State-Mediated Hole Conduction. Adv Energy Mater 2023, 13 (8). https://doi.org/10.1002/aenm.202203183.

(9) Sa, Z.; Liu, F.; Zhuang, X.; Yin, Y.; Lv, Z.; Wang, M.; Zhang, J.; Song, K.; Chen, F.; Yang, Z. Toward High Bias-Stress Stability P-Type GaSb Nanowire Field-Effect-Transistor for Gate-Controlled Near-Infrared Photodetection and Photocommunication. Adv Funct Mater 2023, 33 (38). https://doi.org/10.1002/adfm.202304064.

(10) Green, M. A.; Hishikawa, Y.; Dunlop, E. D.; Levi, D. H.; Hohl-Ebinger, J.; Yoshita, M.; Ho-Baillie, A. W. Y. Solar Cell Efficiency Tables (Version 53). Progress in Photovoltaics: Research and Applications 2019, 27 (1), 3–12. https://doi.org/10.1002/pip.3102.

(11) Ahmadpanah, F. S.; Orouji, A. A.; Gharibshahian, I. Improving the Efficiency of CIGS Solar Cells Using an Optimized P-Type CZTSSe Electron Reflector Layer. Journal of Materials Science: Materials in Electronics 2021, 32 (17), 22535–22547. https://doi.org/10.1007/s10854-021-06740-6.

(12) Todorov, T. K.; Gunawan, O.; Gokmen, T.; Mitzi, D. B. Solution-Processed $Cu(In,Ga)(S,Se)_2$ Absorber Yielding a 15.2% Efficient Solar Cell. Progress in Photovoltaics: Research and Applications 2013, 21 (1), 82–87. https://doi.org/10.1002/pip.1253.

(13) Romanyuk, Y. E.; Hagendorfer, H.; Stücheli, P.; Fuchs, P.; Uhl, A. R.; Sutter-Fella, C. M.; Werner, M.; Haass, S.; Stückelberger, J.; Broussillou, C.; Grand, P. P.; Bermudez, V.; Tiwari, A. N. All Solution-Processed Chalcogenide Solar Cells - From Single Functional Layers Towards a 13.8% Efficient CIGS Device. Adv Funct Mater 2015, 25 (1), 12–27. https://doi.org/10.1002/adfm.201402288.

(14) Awasthi, V.; Pandey, S. K.; Pandey, S. K.; Verma, S.; Gupta, M.; Mukherjee, S. Growth and Characterizations of Dual Ion Beam Sputtered CIGS Thin Films for Photovoltaic Applications. Journal of Materials Science: Materials in Electronics 2014, 25 (7), 3069–3076. https://doi.org/10.1007/s10854-014-1985-0.

(15) Suresh, S.; Uhl, A. R. Present Status of Solution-Processing Routes for $Cu(In,Ga)(S,Se)_2$ Solar Cell Absorbers. Advanced Energy Materials. John Wiley and Sons Inc April 1, 2021. https://doi.org/10.1002/aenm.202003743.

(16) Clark, J. A.; Murray, A.; Lee, J. M.; Autrey, T. S.; Collord, A. D.; Hillhouse, H. W. Complexation Chemistry in N,N-Dimethylformamide-Based Molecular Inks for Chalcogenide Semiconductors and Photovoltaic Devices. J Am Chem Soc 2019, 141 (1), 298–308. https://doi.org/10.1021/jacs.8b09966.

(17) Shannon, R. D. Revised Effective Ionic Radii and Systematic Studies of Interatomic Distances in Halides and Chalcogenides. Acta Crystallographica Section A 1976, 32 (5), 751–767. https://doi.org/10.1107/S0567739476001551.

(18) Maeda, T.; Takeichi, T.; Wada, T. Systematic Studies on Electronic Structures of $CuInSe_2$ and the Other Chalcopyrite Related Compounds by First Principles Calculations. Physica Status Solidi (A) Applications and Materials Science 2006, 203 (11), 2634–2638. https://doi.org/10.1002/pssa.200669539.

(19) Tell, B.; Shay, J. L.; Kasper, H. M. Room-Temperature Electrical Properties of Ten I-III-VI2 Semiconductors. J Appl Phys 1972, 43 (5), 2469–2470. https://doi.org/10.1063/1.1661532.

(20) Mustafa, H.; Hunter, D.; Pradhan, A. K.; Roy, U. N.; Cui, Y.; Burger, A. Synthesis and Characterization of $AgInSe_2$ for Application in Thin Film Solar Cells. Thin Solid Films 2007, 515 (17), 7001–7004. https://doi.org/10.1016/j.tsf.2007.02.054.

(21) Valdes, N.; Lee, J. W.; Shafarman, W. Comparison of Ag and Ga Alloying in Low Bandgap CuInSe 2 -Based Solar Cells. Solar Energy Materials and Solar Cells 2019, 195, 155–159. https://doi.org/10.1016/j.solmat.2019.02.022.

(22) Sopiha, K. V.; Larsen, J. K.; Donzel-Gargand, O.; Khavari, F.; Keller, J.; Edoff, M.; Platzer-Björkman, C.; Persson, C.; Scragg, J. J. S. Thermodynamic Stability, Phase Separation and Ag Grading in $(Ag,Cu)(In,Ga)Se_2$ solar Absorbers. J Mater Chem A Mater 2020, 8 (17), 8740–8751. https://doi.org/10.1039/d0ta00363h.

(23) Abdel-Hady, D.; Salem, A. M. Electrical Resistivity of $AgInSe_2$ Films; Elsevier, 1997; Vol. 242. https://doi.org/10.1016/S0378-4371(97)00200-8.

(24) Arredondo, C. A.; Gordillo, G. Photoconductive and Electrical Transport Properties of $AgInSe_2$ Thin Films Prepared by Co-Evaporation. Physica B Condens Matter 2010, 405 (17), 3694–3699. https://doi.org/10.1016/j.physb.2010.05.068.

(25) Al-Agel, F. A.; Mahmoud, W. E. Synthesis and Characterization of AIS Chalcopyrite Thin Films for Solar Cell Applications. Mater Lett 2012, 82, 82–84. https://doi.org/10.1016/j.matlet.2012.05.065.

(26) Patel, S. M.; Patel, A. D. Electrical resistivity of polycrystalline $AgInSe_2$ thin films. Materials Letters 1983, Vol 2, Issue 2, 127-130. https://doi.org/10.1016/0167-577X(83)90052-6.

(27) Ramesh, P. P.; Naidu, P. J.; Reddy, A. M. A. Optical Absorption Studies on Single-Phase Polycrystalline AglnSe2 Thin Films; 1996.

(28) Matsuo, H.; Yoshino, K.; Ikari, T. Preparation of $AgInSe_2$ Thin Films Grown by Vacuum Evaporation Method. In Physica Status Solidi (C) Current Topics in Solid State Physics; 2006; Vol. 3, pp 2644–2647. https://doi.org/10.1002/pssc.200669511.

(29) Santhosh Kumar, M. C.; Pradeep, B. Formation and Properties of $AgInSe_2$ Thin Films by Co-Evaporation. Vacuum 2004, 72 (4), 369–378. https://doi.org/10.1016/j.vacuum.2003.09.008.

(30) Kaleli, M.; Çolakoğlu, T.; Parlak, M. Production and Characterization of Layer by Layer Sputtered Single-Phase $AgInSe_2$ Thin Film by Thermal Selenization. Appl Surf Sci 2013, 286, 171–176. https://doi.org/10.1016/j.apsusc.2013.09.043.

(31) Scheer, R.; Schock, H. Chalcogenide Photovoltaics; Wiley, 2011. https://doi.org/10.1002/9783527633708.

(32) Nakamura, M.; Yamaguchi, K.; Kimoto, Y.; Yasaki, Y.; Kato, T.; Sugimoto, H. Cd-Free $Cu(In,Ga)(Se,S)_2$ Thin-Film Solar Cell with Record Efficiency of 23.35%. IEEE J Photovolt 2019, 9 (6), 1863–1867. https://doi.org/10.1109/JPHOTOV.2019.2937218.

(33) Walker, B. C.; Agrawal, R. Contamination-Free Solutions of Selenium in Amines for Nanoparticle Synthesis. Chemical Communications 2014, 50 (61), 8331–8334. https://doi.org/10.1039/c4cc02379j.

(34) Rokke, D. Deposition and Characterization of Solution-Processed Chalcogenides for Photovoltaic Applications, Purdue University, 2022.

(35) Guo, Q.; Ford, G. M.; Hillhouse, H. W.; Agrawal, R. Sulfide Nanocrystal Inks for Dense $Cu(In_{1-x}Ga_x)(S_{1-y}Se_y)_2$ Absorber Films and Their Photovoltaic Performance. Nano Lett 2009, 9 (8), 3060–3065. https://doi.org/10.1021/nl901538w.

(36) Kyle Weidemann. Development and Characterization of Film Formation Processes Toward the Improved Performance of Solution-Processed Semiconducting Thin Films. Purdue University 2022.

(37) Erat, S.; Metin, H. Cadmium Sulfide Thin Films Grown By Chemical Bath Deposition Method. In AIP Conference Proceedings; AIP, 2007; pp 599–599. https://doi.org/10.1063/1.2733340.

(38) Pradhan, A. A.; Uible, M. C.; Agarwal, S.; Turnley, J. W.; Khandelwal, S.; Peterson, J. M.; Blach, D. D.; Swope, R. N.; Huang, L.; Bart, S. C.; Agrawal, R. Synthesis of $BaZrS_3$ and $BaHfS_3$ Chalcogenide Perovskite Films Using Single-Phase Molecular Precursors at Moderate Temperatures. Angewandte Chemie International Edition 2023, 62 (15). https://doi.org/10.1002/anie.202301049.

(39) McLeod, S.; Alruqobah, E.; Agrawal, R. Liquid Assisted Grain Growth in Solution Processed $Cu(In,Ga)(S,Se)_2$. Solar Energy Materials and Solar Cells 2019, 195, 12–23. https://doi.org/10.1016/j.solmat.2019.02.020.

(40) Hages, C. J.; Koeper, M. J.; Miskin, C. K.; Brew, K. W.; Agrawal, R. Controlled Grain Growth for High Performance Nanoparticle-Based Kesterite Solar Cells. Chemistry of Materials 2016, 28 (21), 7703–7714. https://doi.org/10.1021/acs.chemmater.6b02733.

(41) Vincent, K. C.; Agarwal, S.; Turnley, J. W.; Agrawal, R. Liquid Flux–Assisted Mechanism for Modest Temperature Synthesis of Large-Grain $BaZrS_3$ and $BaHfS_3$ Chalcogenide Perovskites. Advanced Energy and Sustainability Research 2023, 4 (5). https://doi.org/10.1002/aesr.202300010.

(42) Ammar, A. H.; Farid, A. M.; Seyam, M. A. M. Heat Treatment Effect on the Structural and Optical Properties of $AgInSe_2$ Thin Films. Vacuum 2002, 66 (1), 27–38. https://doi.org/10.1016/S0042-207X(01)00417-1.

(43) Ait Aouaj, M. $AgInSe_2$ Thin Films Prepared by Electrodeposition Process. International Journal of Materials Science and Applications 2015, 4 (1), 35. https://doi.org/10.11648/j.ijmsa.20150401.17.

(44) Essaidi, H.; Gantassi, A.; Touihri, S.; Ouerfelli, J. Tuning the Structural, Optical and Electrical Properties of $AgInSe_2$ Thin Films Prepared by Sequentially Deposited Silver and Indium Nano-Films under Vacuum. Optik (Stuttg) 2019, 182, 866–875. https://doi.org/10.1016/j.ijleo.2018.11.170.

(45) Panda, R.; Panda, M.; Rath, H.; Singh, U. P.; Naik, R.; Mishra, N. C. Annealing Induced $AgInSe_2$ Formation from Ag/In/Ag/In Multilayer Film for Solar Cell Absorbing Layer. Opt Mater (Amst) 2018, 84, 618–624. https://doi.org/10.1016/j.optmat.2018.07.049.

(46) Panda, R.; Khan, S. A.; Singh, U. P.; Naik, R.; Mishra, N. C. The Impact of Fluence Dependent 120 MeV Ag Swift Heavy Ion Irradiation on the Changes in Structural, Electronic, and Optical Properties of $AgInSe_2$ Nano-Crystalline Thin Films for Optoelectronic Applications.

 

RSC Adv 2021, 11 (42), 26218–26227. https://doi.org/10.1039/D1RA03409J.

(47) Pathak, D.; Wagner, T.; Adhikari, T.; Nunzi, J. M. Photovoltaic Performance of $AgInSe_2$-Conjugated Polymer Hybrid System Bulk Heterojunction Solar Cells. Synth Met 2015, 199, 87–92. https://doi.org/10.1016/j.synthmet.2014.11.015.

(48) Zhang, S. B.; Wei, S.-H.; Zunger, A.; Katayama-Yoshida, H. Defect Physics of the $CuInSe_2$ Chalcopyrite Semiconductor. Phys Rev B 1998, 57 (16), 9642–9656. https://doi.org/10.1103/PhysRevB.57.9642.

(49) Ema, Y.; Harakawa, N. Formation and Properties of $AgInSe_2$ Thin Films Deposited from Alloy Chunks. Jpn. J. Appl. Phys. 1995, 34 3260. **DOI** 10.1143/JJAP.34.3260.

(50) Deshmukh, S. D.; Weideman, K. G.; Ellis, R. G.; Kisslinger, K.; Agrawal, R. Enabling Fine-Grain Free 2-Micron Thick CISe/CIGSe Film Fabrication via a Non-Hydrazine Based Solution Processing Route. Mater Adv 2022, 3 (7), 3293–3302. https://doi.org/10.1039/D2MA00095D.

(51) Li, H.; Chen, J.; Zhang, Y.; Wang, W.; Gu, H. Efficiency Enhancement of CIGS Solar Cells via Recombination Passivation. ACS Appl Energy Mater 2020, 3 (9), 9459–9467. https://doi.org/10.1021/acsaem.0c01930.

(52) Green, M. A.; Ho-Baillie, A. W. Y. Pushing to the Limit: Radiative Efficiencies of Recent Mainstream and Emerging Solar Cells. ACS Energy Lett 2019, 4 (7), 1639–1644. https://doi.org/10.1021/acsenergylett.9b01128.

(53) Keller, J.; Sopiha, K. V.; Stolt, O.; Stolt, L.; Persson, C.; Scragg, J. J. S.; Törndahl, T.; Edoff, M. Wide-gap (Ag,Cu)(In,Ga)$Se_2$ Solar Cells with Different Buffer Materials—A Path to a Better Heterojunction. Progress in Photovoltaics: Research and Applications 2020, 28 (4), 237–250. https://doi.org/10.1002/pip.3232.

(54) Stoffel, N. G. Experimental Band Structure of Cadmium Sulfide. Phys Rev B 1983, 28 (6), 3306–3319. https://doi.org/10.1103/PhysRevB.28.3306.

(55) Inceesungvorn, B.; Teeranunpong, T.; Nunkaew, J.; Suntalelat, S.; Tantraviwat, D. Novel $NiTiO_3/Ag_3VO_4$ Composite with Enhanced Photocatalytic Performance under Visible Light. Catal Commun 2014, 54, 35–38. https://doi.org/10.1016/j.catcom.2014.05.015.